THE JOURNAL OF PHYSICAL CHEMISTRY Letters

Letter

pubs.acs.org/JPCL

Polarization Switching and Light-Enhanced Piezoelectricity in Lead Halide Perovskites

Mariona Coll,*[,†] Andrés Gomez,[†] Elena Mas-Marza,[‡] Osbel Almora,[‡] Germà Garcia-Belmonte,[‡] Mariano Campoy-Quiles,[†] and Juan Bisquert*[,‡,§]

[†]Institut de Ciència de Materials de Barcelona (ICMAB-CSIC), Campus UAB, 08193, Bellaterra, Catalonia, Spain

[‡]Photovoltaics and Optoelectronic Devices Group, Departament de Física, Universitat Jaume I, 12071, Castelló, Spain

[§]Department of Chemistry, Faculty of Science, King Abdulaziz University, Jeddah 22254, Saudi Arabia

Supporting Information

ABSTRACT: We investigate the ferroelectric properties of photovoltaic methylammonium lead halide $CH_3NH_3PbI_3$ perovskite using piezoelectric force microscopy (PFM) and macroscopic polarization methods. The electric polarization is clearly observed by amplitude and phase hysteresis loops. However, the polarization loop decreases as the frequency is lowered, persisting for a short time only, in the one second regime, indicating that $CH_3NH_3PbI_3$ does not exhibit permanent polarization at room temperature. This result is confirmed by macroscopic polarization measurement based on a standard capacitive method. We have observed a strong increase of piezoelectric response under illumination, consistent with the previously reported giant photoinduced dielectric constant at low frequencies. We speculate that an intrinsic charge transfer photoinduced dipole in the perovskite cage may lie at the origin of this effect.

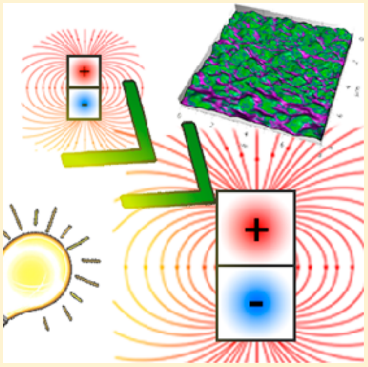

Very high power conversion efficiencies of sunlight to electricity have been obtained for photovoltaic devices based on hybrid inorganic−organic lead halide perovskites in a short time of research.[1−4] Methylammonium lead halide materials as $CH_3NH_3PbI_3$ ($MAPbI_3$) and the associated substitutional variants display excellent photovoltaic properties in terms of light absorption, electronic charge separation, transport and recombination. These materials provide a very promising novel route to massive solution-based facile fabrication of low cost solar cells. However, the chemical and structural properties of the inorganic−organic perovskite, which are unprecedented in the previously known high efficiency photovoltaic materials, produce a number of physical features that are not understood and are intensely investigated at present. In the hybrid perovskite structure ABX_3, the organic cation A^+ is in a cage formed by four BX_6 octahedra. It has become evident that under photovoltaic operation (light or voltage biasing), the "soft" structure of the hybrid perovskite, associated with the combination of organic and inorganic ionic components, produces peculiar and significant phenomena in the ultraslow time regime as current−voltage hysteresis[5,6] and persistent photovoltage decay.[7−9] These properties have been assigned to either ferroelectric or ionic polarization, or else to electronic traps.[10,11] Another connection between structure and electronic response is established by the giant dielectric constant observed in $MAPbI_3$, that is strongly enhanced by illumination. This property has been observed by capacitance spectroscopy[12] and suggests the formation of a large photoinduced dipole.[13]

This paper investigates the ferroelectric polarization that may have a substantial impact on device operation and give rise to novel applications of the inorganic−organic lead halide perovskites in multiferroic materials.[14] In general, many oxide perovskites are highly polar and show a ferroelectric response that provides a static dielectric constant in the order of 10^3. $MAPbI_3$ with tetragonal symmetry belongs to the $4mm$ point group and $I4/mcm$ space group and as such could be ferroelectric. The polarization P in hybrid perovskites may arise from three major mechanisms: the ionic off-centering, the atomic BX_6 cage rotations, and the rotation of dipolar MA^+. The latter mechanism is facile,[15] and it has been favored in recent simulation studies of polarization in $MAPbI_3$,[16−18] as dipole rotation is simpler to treat than cooperative ionic displacements. Former studies,[19,20] both for CH_3NH_3 PbI_3 and $CH_3NH_3PbBr_3$, showed that at room temperature, the PbX_6 octahedra rotate alternatively around the c-axis conforming the $SrTiO_3$-type tetragonal perovskite structure, and the rotation angle of the PbI_6 octahedra increases with decreasing temperature. The transition from tetragonal to orthorhombic phase is accompanied by a peak of the dielectric constant, suggesting that the orthorhombic phase is ferroelectric. More recently, the local dipole structure property has been invoked to explain a giant dielectric constant,[12] slow dynamic response[10] and current−voltage hysteresis.[21,22] However, local polarization

Received: March 10, 2015
Accepted: March 30, 2015
Published: March 30, 2015

DOI: 10.1021/acs.jpclett.5b00502
J. Phys. Chem. Lett. 2015, 6, 1408−1413

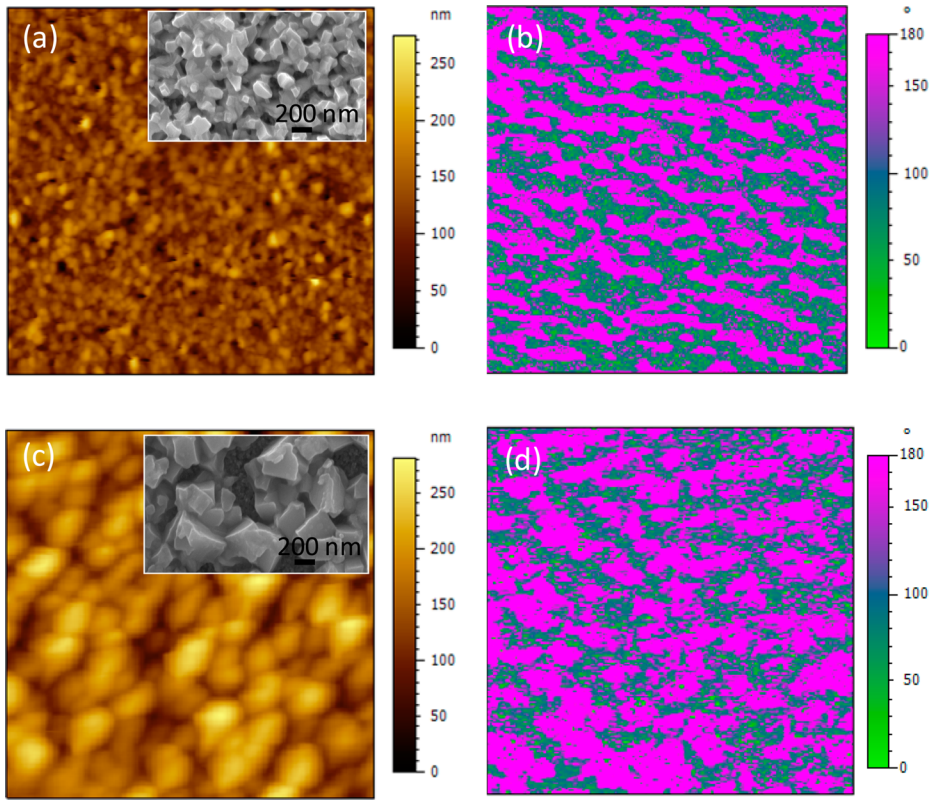

Figure 1. PFM analysis of $MAPbI_3$ films. (a) Topographic and (b) out-of-plane PFM-phase image of $MAPbI_3$ films with small crystals. (c) Topographic and (d) out-of-plane PFM phase image of $MAPbI_3$ films with large crystals. Image size is 8 μm × 8 μm. PFM phase image is in false color. The insets show SEM images of the corresponding samples.

distortion may be combined with long-range ionic drift that establishes macroscopic polarization at the contacts of the sample.[6]

Importantly, there are only a few direct observations of polarization features of inorganic−organic lead halide perovskites, and the results reported so far are not conclusive. One study[23] claimed the direct observation of ferroelectric domains, while another one reported the absence of such effects.[11] Piezoelectric force microscopy (PFM) is a variant of AFM that is widely used to image polarization structure and local switching. However, the observation of contrast region is not sufficient evidence for the existence of ferroic domains, since such contrast may be due to several factors, namely: the existence of ferroelectric domains, electrochemical phenomena, ion migration, electrostatic effects, and it can also have a contribution from surface topography.[24−26] Nevertheless, the states of opposite polarization under applied bias are clearly revealed by a *change of phase* of ac voltage, since the piezoelectric response has different sign in either state of polarization, and this method is shown below. Another important point is whether voltage induced polarization remains permanent, as in ferroelectric material, or disappears when the external voltage is removed.

In order to obtain a clear picture of polarization in $MAPbI_3$, we have investigated polarization switching, the light dependence and the relaxation time in $MAPbI_3$, using PFM and macroscopic polarization measurement. The structure of the samples prepared as indicated in Experimental methods consists of FTO/TiO_2 buffer layer/TiO_2 mesoporous layer (200 nm)/$MAPbI_3$. The samples were measured without upper contact, but their related solar cells provided a power conversion efficiency of about 9% with a photovoltage of ca. 1 V (see SI). Samples with different crystal size have been prepared[27] with the aim to investigate a possible interaction between morphology and polarizability. Topographic images were acquired simultaneously with the PFM-phase images. From the topographic image, the samples with small $MAPbI_3$ crystals display a surface roughness (rms) of 25 nm and an average crystal size diameter of 200 nm (Figure 1a), whereas samples with large $MAPbI_3$ crystals show a rms of 38 nm and a measured crystal size diameter of 500 nm (Figure 1c). This morphological analysis is in good agreement with the scanning electron microscopy (SEM) study as shown in the corresponding inset images.

High humidity conditions (80−90%) can promote the existence of electrochemical phenomena between the tip and the sample surface, which can lead to surface damage and misinterpretation of PFM data.[28] In order to minimize the amount of water layers between the tip and the sample surface and therefore minimize the existence of electrochemical reactions, we performed the experiments under low humidity conditions (<5%). Importantly, careful inspection of the surface topography before and after the acquisition of the PFM image indicates that no undesired topography changes occurred during the PFM measurement.

The PFM-phase images of both samples show a significant phase contrast (see Figure 1b,d). Interestingly, no correlation between the domain shape and location and surface grain morphology was observed (see Figure 1a,c). This suggests a minimal contribution from the surface topography on the PFM-phase contrast image. Qualitative analysis of the two colored areas (false colors), showed that the pink areas results in 38% ±

DOI: 10.1021/acs.jpclett.5b00502
J. Phys. Chem. Lett. 2015, 6, 1408−1413

5 for the small crystal samples and 45% ± 5 for the large crystal samples, Figure 1b and d respectively, which rule out any crystal size dependence. Previous PFM studies on solution-processed $MAPbI_3$ thin films attributed similar piezo-phase contrast to ferroelectric domains.[23] However, it is not straightforward from the PFM phase image to discriminate between charge accumulation and ferroelectric domains;[24] therefore, extra characterization is required. In-field hysteresis loops using a 140 V/s scan rate were obtained by measuring the piezoresponse in the presence of an electric field. Representative locally measured PFM-amplitude and phase loops for both samples are shown in Figure 2. The observed 180° phase switch

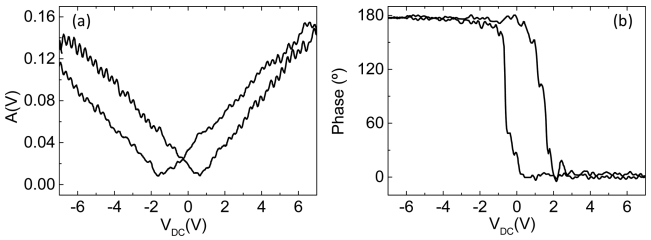

Figure 2. (a) Piezo amplitude and (b) Piezo-phase hysteresis loops of $MAPbI_3$ thin films recorded at a 140 V/s scan rate.

indicates a switchable portion of spontaneous polarization.[29] These results are in contrast to the work published by Xiao et al. where they obtained a flat signal when measuring both the PFM hysteresis loops and the macroscopic ferroelectric polarization loops, using a 0.08 V/s scan rate.[11] One major difference between the two measurements is the scan rates, which might suggest that these halide perovskites present a poor (if any) polarization retention, as we demonstrate below. Remanent loops (measurement in the absence of DC field) further confirmed the lack of ferroelectric retention in MAPI films.

We performed a series of piezo-phase loops in a range of 0.1−10 s acquisition times (corresponding to 140−1.4 V/s scan rates) and analyzed the evolution of the coercivity (see Figure 3a,b). It is clearly observed that the coercivity decays with time

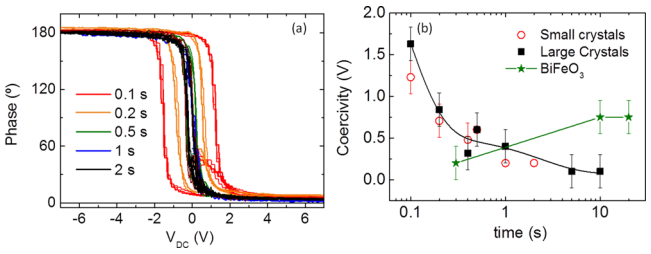

Figure 3. (a) Piezo-phase hysteresis loops of $MAPbI_3$ thin films with small crystals performed at different acquisition times. (b) Coercivity dependence with time of $MAPbI_3$ films with small (red open circles) and large crystals (black squares) and 25 nm $BiFeO_3$ thin films (green stars).

and beyond 1s decreases by a factor of 2. By contrast, the coercivity evolution of a typical ferroelectric perovskite oxide such as $BiFeO_3$ film, increases from 0.3 to 10 s, being retained for several hours and even months.[30] No significant difference in the retention behavior is identified when comparing $MAPbI_3$ samples with small and big crystals, Figure 3b. We next carried out the experiment to electrically write (pole) with the AFM probe an area of 4 μm × 4 μm with −7 V DC bias and then pole back an inner area of 2 μm × μm with +7 DC. When imaging this area, and contrary to the case of well-known ferroelectric materials such as $BiFeO_3$, there is no visible change in the PFM-phase image (see Supporting Information Figure S3). Note that the whole process (writing and reading) takes 8 min to complete, which is much larger than the time scales of the coercivity decay obtained above (Figure 3b). From these data we can confirm that polarization retention in these $MAPbI_3$ films occurs only for very short times.

In order to further corroborate the absence of ferroelectric retention in $MAPbI_3$ films, macroscopic polarization P analyses with respect to electrical field E were carried out using the classical Sawyer−Tower circuit (inset of Figure 4). This

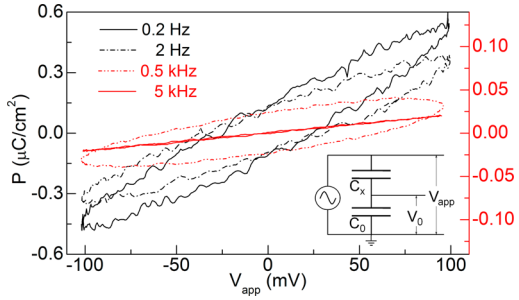

Figure 4. Polarization tests of large crystal $MAPbI_3$-based complete solar cells using the Sawyer−Tower circuit in the inset. At high frequencies, the response is purely capacitive. At low frequencies, elliptic traces indicate the angular phase shift produced by resistive elements.

experiment allows recording hysteresis P−E loops by polarizing the sample and registering the induced charge in the plates of a reference capacitor. We used the testing circuit to explore the existence of ferroelectric hysteresis loops with large crystal $MAPbI_3$-based complete solar cells using *spiro*-OMeTAD/Au top contacts. When high-frequencies are used in the polarizing voltage source (5 kHz) only purely capacitive responses are obtained as observed in Figure 4b. Since piezo-phase loops in Figure 3a show coercivity decay in the range of seconds, low-frequency P−E loops were also checked. As shown in Figure 4, only linear responses (ellipses) are obtained. These loops occur as a consequence of the series connection of resistive and capacitive elements. Importantly, the resistance introduces a time delay that tends to disappear as the perturbation frequency is reduced. In agreement with our previous PFM analysis, ferroelectric features were not found by macroscopic polarization tests in $MAPbI_3$ films.

In another set of experiments, we investigated the PFM response of $MAPbI_3$ films under illumination with white light from a LED with 4.5 mW power (PFM setup shown in the Supporting Information, Figure S5). Under such conditions, we observed no change in the piezo-phase hysteresis loops, nor in the retention times.

The effective piezoelectric coefficient of the $MAPbI_3$ films, d_{zz}, was derived from the linear dependence between an averaged tip oscillation amplitude A according to $A = d_{zz}V_{AC}$,[31] obtaining 5 pm/V and 6 pm/V for the small and large crystal samples, respectively (see Supporting Information Figure S2). To the best of our knowledge, there are no examples in the literature regarding theoretical values of the piezoelectric coefficient of perovskite halides. As a reference, values between

DOI: 10.1021/acs.jpclett.5b00502
J. Phys. Chem. Lett. 2015, 6, 1408−1413

10 and 50 pm/V are typically reported for 0.2−0.6 μm nm lead zirconate titanate (PZT) ferroelectric films.[32]

Interestingly, we also measured the effective piezoelectric coefficient under white light and found that it dramatically increased up to 25 pm/V (see Figure 5a). Note that the

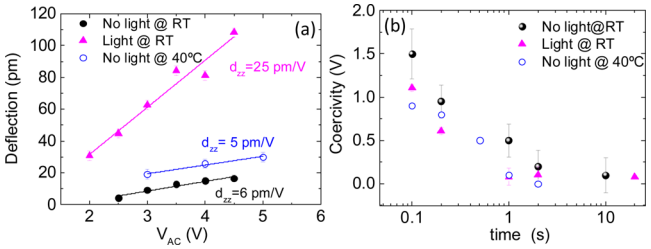

Figure 5. (a) Deflection versus V_{AC} and (b) coercivity dependence with time for $MAPbI_3$ films in the dark at room temperature (RT) (black circles), under illumination (pink triangles) and in dark and at 40 °C (blue open circles).

observed increase in the d_{zz} coefficient under illumination is in sharp contrast with the results of previous studies[33,34] performed on ferroelectric PZT films, where it was observed that the UV light (under weak electric filed) induced a decrease in the piezoelectric coefficient explained by a reduction of the overall polarization. The magnitude of the bulk polarization of $MAPbI_3$ has been predicted to be 38 $\mu C/cm^2$ based on the molecular dipole moment 2.29 D of the cation MA^+.[16,35] However, the dielectric constant increases strongly at low frequencies, and furthermore a photoinduced giant dielectric constant has been observed in $MAPbI_3$ films.[12] An internal charge transfer transition upon light excitation may lead to a large added dipole moment. By means of modulation electroabsorption (EA) spectroscopy, Wu et al.[13] calculated a change of the electronic dipole moment, $\Delta\mu$, (from ground state to excited state) of 288 D, which is notably larger than the change observed in other widely studied photosensitive materials such as CdSe ($\Delta\mu \sim 20-30$ D). Therefore, the impressive increase in the d_{zz} coefficient identified by PFM under illumination (Figure 5a) can also be related to the formation of large photoinduced dipole moments, in agreement with previous observations by different experimental techniques.

We would like to note again that when measuring the coercivity under illumination with different scanning rates, no differences were observed from the measurements performed in dark (see Figure 5b). Therefore, although the piezoelectric coefficient is 4 times larger, the kinetics under illumination follows the same trend as in dark, i.e., small retention (< 2s).

PFM measurements were also performed on a photosensitive organic material, namely, region regular poly(3-hexyl thiophene) blended with fullerene soluble derivative (PCBM), where no piezoelectric/ferroelectric behavior is expected. Reassuringly, we did not observe PFM domains, nor the typical phase and amplitude loops (see Supporting Information, Figure S4e,g). Consequently, by comparing the PFM behaviors obtained for these two photovoltaic materials, we suggest that the PFM response exhibited by $MAPbI_3$ films is unlikely due to charge accumulation effects arising from photogenerated charges.

Finally, we have also investigated the influence of temperature (RT, 40 °C, 60 °C) on the polarization in order to rule out any temperature-dominated phenomena in the piezoresponse signal. No changes in the domain features were identified in the PFM phase image when exposed to temperatures up to 50 °C (see Supporting Information Figure S6). Considering that no phase transition would be expected at temperatures <60 °C,[36] the coercivity evolution with time and piezoelectric coefficient were evaluated at 40 °C (see Figure 5). The film behaves in the same way at 40 °C as at room temperature in terms of domain sizes, coercivity, and retention times. This fact rules out temperature-related artifacts on the light-induced piezoelectric coefficient increase demonstrated above.

In summary, $MAPbI_3$ films with a TiO_2 contact have been investigated by PFM. The films show large polarizability. Polarization is confirmed by piezo-phase loops that are reported here for the first time. However, at room temperature, $MAPbI_3$ in tetragonal phase has poor polarization retention and it is not ferroelectric. In fact, the coercitivity decays in the time regime of seconds, which is in agreement with the recent interpretation of structural relaxation in photovoltage decays.[8] In addition, we have observed a strong increase of the piezoelectricity when carriers are photogenerated in the $MAPbI_3$ film, which correlates to a previous observation of a photoinduced giant dielectric constant. This observation points to an intrinsic nature of voltage induced polarization in $MAPbI_3$ film, in the sense that the polarization is local and caused by rotation of dipoles or other structural units, with the formation of polarized domains with relatively slow depolarization times. Such local units, so far unidentified, may be strongly enhanced in the presence of photogenerated carriers. However, ion motion still forms a source of "extrinsic" polarization, located at contacts and dependent on sample configuration, and both types of polarization effect may take place depending on sample type.

EXPERIMENTAL METHODS

Solvents and reagents are commercially available and were used as received from commercial suppliers. CH_3NH_3I was synthesized by the reaction of 0.273 mol of a solution of CH_3NH_2 in ethanol with 0.223 mol of aqueous HI, at 0 °C for 4 h. Then, the volatile compounds were removed under reduced pressure; the resulting CH_3NH_3I was recrystallized from ethanol/diethyl ether and dried under vacuum overnight.

$CH_3NH_3PbI_3$ ($MAPbI_3$) Perovskite Films Preparation. Fluorine-doped tin oxide (FTO) coated glass sheets (2.5 × 2.5 mm, Pilkington TEC15, ∼ 15Ω/sq resistance) were cleaned with soap (Hellmanex) and rinsed with Milli-Q water and ethanol. Then, the sheets were sonicated for 15 min in a solution of acetone:isopropanol (1:1 v/v), rinsed with ethanol, and dried with compressed air. After that, a UV/ozone treatment was performed for 15 min. Then, a compact TiO_2 blocking layer was deposited onto the substrates by spray pyrolysis at 450 °C, using a titanium diisopropoxide bis(acetylacetonate) (75% in isopropanol, Sigma-Aldrich) solution diluted in ethanol (1:39, v/v), with oxygen as carrier gas. Then, the films were kept at 450 °C for 5 min. A UV/ozone treatment was performed for 15 min. On top of the compact layer, a 200 nm-thick mesoporous TiO_2 layer was deposited by spin coating at 4000 rpm for 30 s using a TiO_2 paste (Dyesol 18NRT, 20 nm average particle size) diluted in terpineol (1:3, weight ratio). After drying at 80 °C for 10 min, the TiO_2 layers were annealed at 470 °C for 30 min and cooled to room temperature. The mesoporous layer was further treated with 20 mM of aqueous $TiCl_4{\cdot}(THF)_2$ solution at 70 °C for 10 min, and annealed at 500 °C during 30 min. After a UV/ozone treatment for 15 min, 30 μL of a 1.082

DOI: 10.1021/acs.jpclett.5b00502
J. Phys. Chem. Lett. 2015, 6, 1408−1413

M solution of PbI_2 in dimethylformamide was spin-coated onto the mesoporous layer at 500 rpm for 5 s and 6000 rpm for 20 s, followed by heating at 40 °C for 3 min and 100 °C for 10 min on a hot plate. The PbI_2 film was then dipped for 1 min in a solution of CH_3NH_3I in isopropanol (0.044 M for large crystal size and 0.063 M for small crystal size), spun at 500 rpm for 5 s, 1500 rpm for 10 s, and 3000 rpm for 20 s, and heated at 40 °C for 3 min and at 100 °C for 10 min on a hot plate.

$BiFeO_3$ was grown by atomic layer deposition at 250 °C and post annealed at 650 °C (unpublished results). Regioregular poly(3-hexylthiophene) and PCBM were purchased from Sigma-Aldrich and used as received. Films were prepared by knife coating a 30 mg/mL solution in chlorobenzene on top of a 40 nm thick PEDOT:PSS-coated ITO glass substrate.

Piezoelectric Force Microscopy (PFM) Measurement. PFM measurements were performed with an Agilent 5500LS instrument using a rmn-25pt300 tip with a spring constant of 18 N/m. Measurement conditions were kept in a ambient humidity below 5%. PFM measurements were performed in dark and under illumination (4.5 mW). The AC frequency was set to ≈122 kHz, and its amplitude to 0.5 V. The cantilever deformation has been calibrated using a force−distance curve. The effective piezoelectric coefficient of the MAPI film, d_{zz}, was derived from the linear dependence between an averaged tip oscillation amplitude A according to $A = d_{zz}V_{AC}$.

PFM under Illumination. To perform these measurements, we have designed a PFM sample holder made of copper where we can shine light from the bottom using a LED integrated within the holder (see Figure S5). Sample temperature under illumination was measured using a PT1000 sensor at three different sample locations being the typical values all around 22 °C.

PFM at 40−60 °C. The heating was performed using a constant current source connected to a ceramic heater. To measure the temperature, we used a PT1000 sensor located at 1 mm apart from the sample's backside. After acquiring the images, the topside temperature of the sample was measured using another PT1000 sensor to ensure a correct assignment of the surface's temperature, and a 13° difference was found. Temperatures described in the manuscript are already the surface temperature. Macroscopic polarization loops were investigated by means of the classical Sawyer−Tower circuit (inset Figure 4) in which a voltage source polarizes the series connection of the investigated sample and a reference capacitor C_0. The charge induced in the sample was monitored by means of the potential drop at the capacitor as $P = C_0V_0$. For high enough reference capacitor values, the bias voltage mainly drops at the sample.

Structural Characterization. The morphology and structural properties of the films were analyzed using a JEOL 7001F scanning electron microscope with a film emission gun (SEMFEG). Phase purity and film crystallinity were studied by using a GADDS X-ray diffractometer equipped with a 2D X-ray detector with Cu−K_α λ = 1.5418 Å (see Supporting Information Figure S1).

■ ASSOCIATED CONTENT

Supporting Information

Additional figures and details as decribed in the text. This material is available free of charge via the Internet http://pubs.acs.org.

■ AUTHOR INFORMATION

Corresponding Authors

*E-mail: mcoll@icmab.es (M.C.).
*E-mail: jbisquert@uji.es (J.B.).

Notes

The authors declare no competing financial interest.

■ ACKNOWLEDGMENTS

We acknowledge financial support from the Spanish Ministerio de Economía y Competitividad (MINECO) through RyC contracts 2013-12448 and 2011-07726 and projects MAT2013-47192-C3-1-R and MAT2012-37776. We thank Sang-Woo Kim and Ignasi Fina for fruitful discussions.

■ REFERENCES

(1) Kojima, A.; Teshima, K.; Shirai, Y.; Miyasaka, T. Organometal Halide Perovskites as Visible-Light Sensitizers for Photovoltaic Cells. *J. Am. Chem. Soc.* **2009**, *131*, 6050−6051.

(2) Kim, H.-S.; Lee, C.-R.; Im, J.-H.; Lee, K.-B.; Moehl, T.; Marchioro, A.; Moon, S.-J.; Humphry-Baker, R.; Yum, J.-H.; Moser, J. E.; et al. Lead Iodide Perovskite Sensitized all-Solid-State Submicron Thin Film Mesoscopic Solar Cell with Efficiency Exceeding 9%. *Sci. Rep.* **2012**, *2*, 591.

(3) Lee, M. M.; Teuscher, J.; Miyasaka, T.; Murakami, T. N.; Snaith, H. J. Efficient Hybrid Solar Cells Based on Meso-Superstructured Organometal Halide Perovskites. *Science* **2012**, *338*, 643−647.

(4) Jeon, N. J.; Noh, J. H.; Yang, W. S.; Kim, Y. C.; Ryu, S.; Seo, J.; Seok, S. I. Compositional Engineering of Perovskite Materials for High-Performance Solar Cells. *Nature* **2015**, *517*, 476−480.

(5) Snaith, H. J.; Abate, A.; Ball, J. M.; Eperon, G. E.; Leijtens, T.; Noel, N. K.; Stranks, S. D.; Wang, J. T.-W.; Wojciechowski, K.; Zhang, W. Anomalous Hysteresis in Perovskite Solar Cells. *J. Phys. Chem. Lett.* **2014**, *5*, 1511−1515.

(6) Unger, E. L.; Hoke, E. T.; Bailie, C. D.; Nguyen, W. H.; Bowring, A. R.; Heumuller, T.; Christoforo, M. G.; McGehee, M. D. Hysteresis and Transient Behavior in Current-Voltage Measurements of Hybrid-Perovskite Absorber Solar Cells. *Energy Environ. Sci.* **2014**, *7*, 3690−3698.

(7) Baumann, A.; Tvingstedt, K.; Heiber, M. C.; Vath, S.; Momblona, C.; Bolink, H. J.; Dyakonov, V. Persistent Photovoltage in Methylammonium Lead Iodide Perovskite Solar Cells. *APL Mater.* **2014**, *2*, 081501.

(8) Bertoluzzi, L.; Sanchez, R. S.; Liu, L.; Lee, J.-W.; Mas-Marza, E.; Han, H.; Park, N.-G.; Mora-Sero, I.; Bisquert, J. Cooperative Kinetics of Depolarization in $CH_3NH_3PbI_3$ Perovskite Solar Cells. *Energy Environ. Sci.* **2015**, *8*, 910−915.

(9) Pockett, A.; Eperon, G. E.; Peltola, T.; Snaith, H. J.; Walker, A. B.; Peter, L. M.; Cameron, P. J. Characterization of Planar Lead Halide Perovskite Solar Cells by Impedance Spectroscopy, Open Circuit Photovoltage Decay and Intensity-Modulated Photovoltage/Photocurrent Spectroscopy. *J. Phys. Chem. C* **2015**, *119*, 3456−3465.

(10) Sanchez, R. S.; Gonzalez-Pedro, V.; Lee, J.-W.; Park, N.-G.; Kang, Y. S.; Mora-Sero, I.; Bisquert, J. Slow Dynamic Processes in Lead Halide Perovskite Solar Cells. Characteristic Times and Hysteresis. *J. Phys. Chem. Lett.* **2014**, *5*, 2357−2363.

(11) Xiao, Z.; Yuan, Y.; Shao, Y.; Wang, Q.; Dong, Q.; Bi, C.; Sharma, P.; Gruverman, A.; Huang, J. Giant Switchable Photovoltaic Effect in Organometal Trihalide Perovskite Devices. *Nat. Mater.* **2015**, *14*, 193−198.

(12) Juarez-Perez, E. J.; Sanchez, R. S.; Badia, L.; Garcia-Belmonte, G.; Kang, Y. S.; Mora-Sero, I.; Bisquert, J. Photoinduced Giant Dielectric Constant in Lead Halide Perovskite Solar Cells. *J. Phys. Chem. Lett.* **2014**, *5*, 2390−2394.

(13) Wu, X.; Yu, H.; Li, L.; Wang, F.; Xu, H.; Zhao, N. Composition-Dependent Light-Induced Dipole Moment Change in Organometal Halide Perovskites. *J. Phys. Chem. C* **2014**, *119*, 1253−1259.

DOI: 10.1021/acs.jpclett.5b00502
J. Phys. Chem. Lett. 2015, 6, 1408−1413

(14) Kim, M.; Im, J.; Freeman, A. J.; Ihm, J.; Jin, H. Switchable $S = 1/2$ and $J = 1/2$ Rashba Bands in Ferroelectric Halide Perovskites. *Proc. Natl. Acad. Sci. U.S.A.* **2014**, *111*, 6900−6904.
(15) Poglitsch, A.; Weber, D. Dynamic Disorder in Methylammoniumtrihalogenoplumbates (II) Observed by Millimeter Wave Spectroscopy. *J. Chem. Phys.* **1987**, *87*, 6373−6378.
(16) Frost, J. M.; Butler, K. T.; Brivio, F.; Hendon, C. H.; van Schilfgaarde, M.; Walsh, A. Atomistic Origins of High-Performance in Hybrid Halide Perovskite Solar Cells. *Nano Lett.* **2014**, *14*, 2584−2590.
(17) Frost, J. M.; Butler, K. T.; Walsh, A. Molecular Ferroelectric Contributions to Anomalous Hysteresis in Hybrid Perovskite Solar Cells. *APL Mater.* **2014**, *2*, 081506.
(18) Liu, S.; Zheng, F.; Koocher, N. Z.; Takenaka, H.; Wang, F.; Rappe, A. M. Ferroelectric Domain Wall Induced Band-Gap Reduction and Charge Separation in Organometal Halide Perovskites. *J. Phys. Chem. Lett.* **2015**, *6*, 693−699.
(19) Kawamura, Y.; Mashiyama, H.; Hasebe, K. Structural Study on Cubic-Tetragonal Transition of $CH_3NH_3PbI_3$. *J. Phys. Soc. Jpn.* **2002**, *71*, 1694−1697.
(20) Mashiyama, H.; Magome, E.; Kawamura, Y.; Kubota, Y. Displacive Character of the Cubic-Tetragonal Transition in $CH_3NH_3PbX_3$. *J. Korean Phys. Soc.* **2003**, *42*, 1026−1029.
(21) Wei, J.; Zhao, Y.; Li, H.; Li, G.; Pan, J.; Xu, D.; Zhao, Q.; Yu, D. Hysteresis Analysis Based on the Ferroelectric Effect in Hybrid Perovskite Solar Cells. *J. Phys. Chem. Lett.* **2014**, 3937−3945.
(22) Chen, H.-W.; Sakai, N.; Ikegami, M.; Miyasaka, T. Emergence of Hysteresis and Transient Ferroelectric Response in Organo-Lead Halide Perovskite Solar Cells. *J. Phys. Chem. Lett.* **2014**, *6*, 164−169.
(23) Kutes, Y.; Ye, L. H.; Zhou, Y. Y.; Pang, S. P.; Huey, B. D.; Padture, N. P. Direct Observation of Ferroelectric Domains in Solution-Processed $CH_3NH_3PbI_3$ Perovskite Thin Films. *J. Phys. Chem. Lett.* **2014**, *5*, 3335−3339.
(24) Balke, N.; Maksymovych, P.; Jesse, S.; Kravchenko, I.; Li, Q.; Kalinin, S. Exploring Local Electrostatic Effects with Scanning Probe Microscopy: Implications for Piezoresponse Force Microscopy and Triboelectricity. *ACS Nano* **2014**, *8*, 10229−10236.
(25) Kalinin, S.; Kumar, A.; Balke, N.; McCorkle, M.; Guo, S. L.; Arruda, T.; Jesse, S. ESM of Ionic and Electrochemical Phenomena on the Nanoscale. *Adv. Mater. Process* **2011**, *169*, 30−34.
(26) Kalinin, S. V.; Jesse, S.; Tselev, A.; Baddorf, A. P.; Balke, N. The Role of Electrochemical Phenomena in Scanning Probe Microscopy of Ferroelectric Thin Films. *ACS Nano* **2011**, *5*, 5683−5691.
(27) Im, J.-H.; Jang, I.-H.; Pellet, N.; Grätzel, M.; Park, N.-G. Growth of $CH_3NH_3PbI_3$ Cuboids with Controlled Size for High-Efficiency Perovskite Solar Cells. *Nat. Nano.* **2014**, *9*, 927−932.
(28) Dahan, D.; Molotskii, M.; Rosenman, G.; Rosenwaks, Y. Ferroelectric Domain Inversion: The Role of Humidity. *Appl. Phys. Lett.* **2006**, *89*, 152902.
(29) Lines, M. E.; Glass, A. M. *Principles and Applications of Ferroelectrics and Related Materials*; Clarendon Press: Oxford, 2001.
(30) Bea, H.; Ziegler, B.; Bibes, M.; Barthelemy, A.; Paruch, P. Nanoscale Polarization Switching Mechanisms in Multiferroic $BiFeO_3$ Thin Films. *J. Phys.: Condens. Matter* **2011**, *23*, 142201.
(31) Kalinin, S. V.; Rodriguez, B. J.; Jesse, S.; Shin, J.; Baddorf, A. P.; Gupta, P.; Jain, H.; Williams, D. B.; Gruverman, A. Vector Piezoresponse Force Microscopy. *Microsc. Microanal.* **2006**, *12*, 206−220.
(32) Lefki, K.; Dormans, G. J. M. Measurement of Piezoelectric Coefficients of Ferroelectric Thin Films. *J. Appl. Phys.* **1994**, *76*, 1764−1767.
(33) Kholkin, A. L.; Iakovlev, S. O.; Baptista, J. L. Direct Effect of Illumination on Ferroelectric Properties of Lead Zirconate Titanate Thin Films. *Appl. Phys. Lett.* **2001**, *79*, 2055−2057.
(34) Kholkin, A. L.; Setter, N. Photoinduced Poling of Lead Titanate Zirconate Thin Films. *Appl. Phys. Lett.* **1997**, *71*, 2854−2856.
(35) Zheng, F.; Takenaka, H.; Wang, F.; Koocher, N. Z.; Rappe, A. M. First-Principles Calculation of the Bulk Photovoltaic Effect in $CH_3NH_3PbI_3$ and $CH_3NH_3PbI_{3-x}Cl_x$. *J. Phys. Chem. Lett.* **2015**, *6*, 31−37.
(36) Baikie, T.; Fang, Y.; Kadro, J. M.; Schreyer, M.; Wei, F.; Mhaisalkar, S. G.; Graetzel, M.; White, T. J. Synthesis and Crystal Chemistry of the Hybrid Perovskite $(CH_3NH_3)PbI_3$ for Solid-State Sensitised Solar Cell Applications. *J. Mater. Chem. A* **2013**, *1*, 5628−5641.

DOI: 10.1021/acs.jpclett.5b00502
J. Phys. Chem. Lett. 2015, 6, 1408−1413